

Self-Similar Micron-Size and Nanosize Drops of Liquid Generated by Surface Acoustic Waves

Daniel Taller,¹ David B. Go,¹ and Hsueh-Chia Chang^{2,*}

¹Department of Aerospace and Mechanical Engineering, University of Notre Dame, Notre Dame, Indiana 46556, USA

²Department of Chemical and Biomolecular Engineering, Center for Microfluidics & Medical Diagnostics, University of Notre Dame, Notre Dame, Indiana 46556, USA

(Received 13 September 2012; published 27 November 2012)

A planar surface acoustic wave on a solid substrate and its radiated sound into a static liquid drop produce time-averaged, exponentially decaying acoustic and electric Maxwell pressures near the contact line. These localized contact-line pressures are shown to generate two sequences of hemispherical satellite droplets at the tens of microns and submicron scales, both obeying self-similar exponential scaling but with distinct exponents that correspond to viscous dissipation and field leakage length scales, respectively. The acoustic pressure becomes dominant when the film thickness exceeds $(1/4\pi)$ of the surface acoustic wave wavelength and it affects the shape and stability of the mother drop. The Maxwell pressure of the nanodrops, which exceeds ten atmospheres, is sensitive to the contact angle.

DOI: 10.1103/PhysRevLett.109.224301

PACS numbers: 43.35.Pt, 68.35.Iv, 78.67.Tf

Surface acoustic waves (SAWs) are elastic compression surface waves generated on piezoelectric crystals by alternating current (ac) electric fields sustained by an interdigitated electrode transducer [1–3]. Both compression and electric traveling waves of specific wavelength can be generated on the surface of the crystal. Like plasmonic optical surface waves, SAWs are dispersive [4], but unlike optical waves, they are highly nonlinear [5]. Surface acoustic compression waves involve nanometer high deformation on the solid and have in-phase [6] electric components. Historically, SAW devices have found widespread use as filters, oscillators, and transformers in the electronics industry [2]. More recently, they have been incorporated into microfluidic devices, where they can be used to manipulate fluids on the surface of the SAW device or disperse fluid into aerosols, with applications ranging from mass spectrometry [6–8] to pulmonary drug delivery [9,10]. Extensive studies have been undertaken to characterize breakup of liquid drops by SAWs [11,12] to generate jets [13,14] and aerosols [15,16].

Microfluidic and mass spectrometry applications are particularly intriguing, as they involve the scattering of the surface wave into a drop or film on the substrate. This scattering is like optical refraction, but the wedge-shaped geometry of the drop at the scattering location (contact line) suggests an electric hot spot similar to a plasmonic hot spots or singular scattering near the tip of a wedge [17,18]. Since the SAW wavelength ($\lambda_{\text{SAW}} \approx 132 \mu\text{m}$) is much larger than the scattering region, an “electrostatic” approximation is permissible for the acoustic wave equation to yield a quasistatic analysis of the acoustic field near the contact line, as is commonly done for the Maxwell wave equation for optics [6,17].

It is indeed known that the acoustic waves that scatter into a bulk drop or a liquid film will generate high acoustic pressure at the contact line [19]. This acoustic radiation

pressure can drive a dc streaming flow that is suspected to be responsible for a contact line instability that pulls a thin film of liquid away from the bulk and causes rupture [20]. However, the time-averaged system can also remain at equilibrium, and the acoustic pressure can be compensated by capillary pressure resulting in a quasistatic equilibrium [20].

While the scattered sound waves produce an acoustic pressure in the bulk liquid, the traveling electric field of the transmitted SAW on the piezoelectric substrate can produce dielectric polarization at the solid-liquid interface with a corresponding electric Maxwell pressure. The singular Laplace harmonics at geometric singularities [21–25] also suggest that the electric traveling wave will generate an electric field maximum (or singularity) near the contact line, which could be responsible for the ionization observed in SAW mass spectrometry. It follows that the SAW-induced Maxwell pressure can also balance the capillary pressure to generate similar small satellite droplets at the contact line or even quasistatic cones, albeit at a shorter length scale since the Maxwell pressure is expected to be shorter range than the acoustic pressure. This balance of electric and capillary pressures at the contact line is analogous to dc Taylor and ac electrospray cones, where an electric Maxwell pressure is balanced by the capillary pressure so that both vary toward infinity in the same manner approaching the cone tip [22,25]. In fact, previous experimental and numerical studies of SAWs along wedge-shaped channels show both high acoustic and electric fields at the tip of the wedge [26,27].

In the present Letter, we experimentally confirm the presence of these effects for the first time and offer scaling theories to clarify where the acoustic and Maxwell pressures dominate. For the quasistatic structures to exist, it is important that the drop does not move under the influence of the SAW. As such, we generate pinned stationary drops

by extracting small amounts ($\sim 0.1 \mu\text{L}$) of liquid onto a SAW device via a paper wick such that the drop is constrained by contact with the paper.

The SAW device for the present study was fabricated using standard photolithographic methods on a 127.68° yx -cut lithium niobate (LiNbO_3) substrate. The SAW device was fabricated with focusing electrodes as pioneered by Wu *et al.* [28] and used in previous studies of SAW for mass spectrometry and microfluidics [6,7]. A small plastic weigh boat was used as a reservoir to supply the working fluid, deionized (DI) water. Cleanroom paper (TX 609 TechniCloth Non Woven Wipers) was used to wick the working fluid onto the substrate so that fluid could be supplied continuously. For all experiments, an ac voltage was applied to the SAW transducers via a waveform generator (Agilent 33250A) attached to an amplifier (E&I 325LA) at a frequency of $f_{\text{SAW}} = 29.5$ MHz. Prior to operation, the paper wick was saturated with fluid from the reservoir and brought to the edge of the SAW device. Upon the application of ac power, SAWs were generated and liquid was drawn from the saturated paper onto the device surface, and at sufficient power aerosolized. This was filmed using a high-speed camera (Photron Fastcam SA4) with a Navitar telescopic lens ($\sim 48 \times$ magnification) adjacent to the SAW device. A schematic of the SAW device and placement of the paper wick is shown in Fig. 1(a).

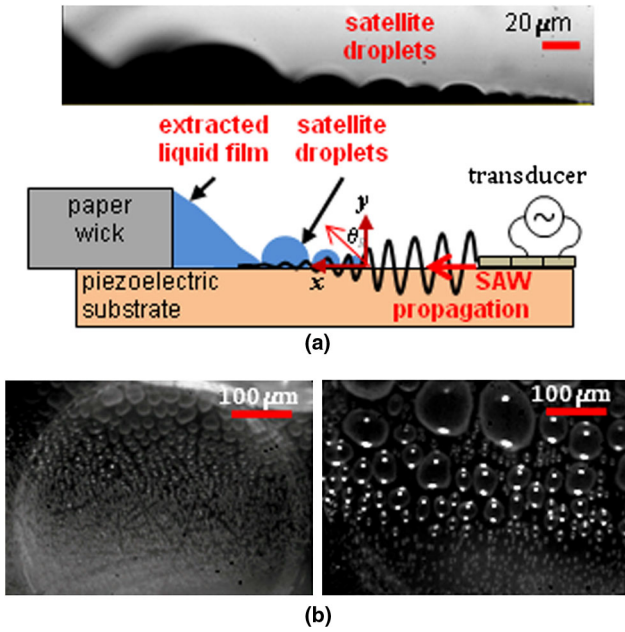


FIG. 1 (color online). (a) Schematic of SAW device producing a droplet train from a pinned liquid film (side view) with inset showing an experimental image of the droplet train using DI water. The acoustic waves refract into the fluid at Rayleigh angle θ_R . (b) Top view of surface droplets for contact angles 45° (left) and 80° (right). Note that the Maxwell droplets decay much more quickly in the image on the right due to the change in contact angle.

At low powers, prior to the onset of aerosolization, a liquid film was extracted from the paper by SAWs and a sequence of self-similar satellite droplets formed on the substrate, as discussed above and shown in Fig. 1(a). The substrate was either cleaned with acetone or was treated with trichloro(1H,1H,2H,2H-perfluorooctyl)silane via evaporation to change the liquid contact angle. The droplets increase in radius closer to the paper wick, which is along the direction of SAW propagation (x coordinate), and the sequence of droplet sizes has a strong dependence on the contact angle [Fig. 2(b)].

We model the droplet size distribution as a train of hemispherical droplets whose radii are controlled by the acoustic or Maxwell pressure that decays into the liquid. The n th hemisphere thus has radius R_n , with position $L_n = 2 \sum_{m=1}^n R_m$, so that the smallest droplet of radius R_1 begins at $L_0 = 0$, the next droplet begins at $L_1 = 2R_1$, and so on. Assuming that the droplet radius R_n is governed by the applied pressure at L_{n-1} , given by $P_{\text{SAW}}(L_{n-1})$, a balance of capillary pressure and the acoustic or Maxwell pressure requires that $2\gamma/R_n = P_{\text{SAW}}(L_{n-1})$, where γ is surface tension. Hence,

$$L_n = 4\gamma \sum_{m=1}^n \frac{1}{P_{\text{SAW}}(L_{m-1})}. \quad (1)$$

In the case that acoustic pressure is dominant, P_{SAW} is due to viscous dissipation of a bulk acoustic wave that refracts off the substrate at an angle corresponding to the Rayleigh scattering angle when the SAW enters into the liquid. The leading-order theory for the propagation and viscous attenuation of the sound wave produces a fluid displacement velocity u_1 with zero time average. However, the time averaged Bernoulli dynamic pressure, $\langle \rho u_1^2/2 \rangle$, where ρ is the ambient equilibrium density, is nonzero and produces a time-averaged acoustic radiation pressure [9,19],

$$P_{\text{acoustic}} = \frac{1}{2} \rho (1 + \alpha^2) A^2 \omega^2 e^{-2(k_x x + k_y y)}, \quad (2)$$

which decays exponentially into the fluid in the same direction of propagation as the velocity u_1 with a characteristic decay length of $l_R = 1/2k_R$. The Rayleigh acoustic decay constant k_R is in the direction of the Rayleigh refraction angle θ_R from the normal, as shown in Fig. 1(a), and has components $k_x = k_R \sin(\theta_R)$ and $k_y = k_R \cos(\theta_R)$, where the Rayleigh angle is $\theta_R = \sin^{-1}(V_w/V_R)$ using Snell's law for the refracted liquid sound wave velocity V_w and the SAW Rayleigh wave velocity V_R . The parameter $\omega = 2\pi f_{\text{SAW}}$ is the angular frequency, A is the amplitude of the SAW, and $\alpha^2 = \cot^2(\theta_R) = (V_R/V_w)^2 - 1$ is an attenuation constant arising from the change in speed of the wave from the solid to the liquid phase.

The radiation pressure (2) can sometimes drive a streaming flow and is hence referred to as a streaming pressure. However, for a thin film, it can be balanced quasistatically

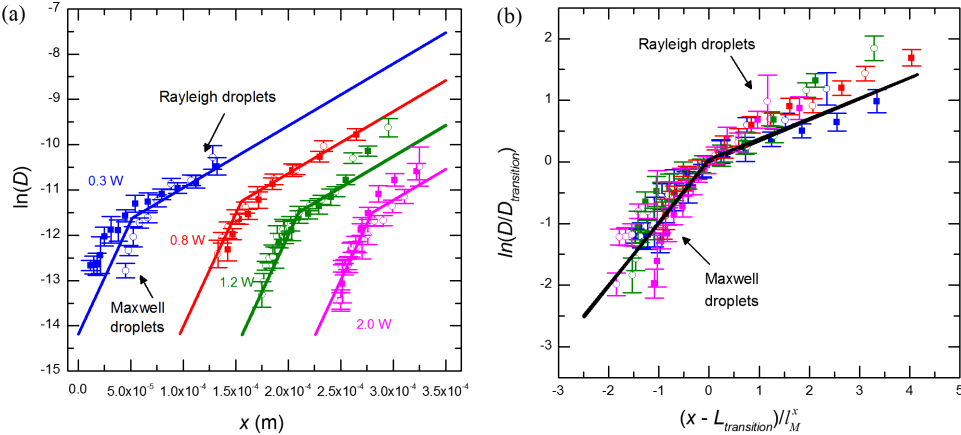


FIG. 2 (color online). (a) Plot of $\ln(D)$ as a function of x for data acquired at different SAW powers along with linear curve fits. All units are in meters and $\theta_c = 45^\circ$ for the untreated substrate. The slopes of the linear fits are equivalent to the decay constant. (b) The data sets collapsed on a single plot, where $D_{\text{transition}}$ is the droplet size where the transition for the two droplet families occurs ($\approx 11 \mu\text{m}$), $L_{\text{transition}}$ is the measured x location of the transition, and l_M^x is the decay length of the Maxwell pressure. Two sets of data (open and closed symbols) were acquired for each power setting.

by an interfacial capillary pressure and a pressure field within the film without generating a dc flow. This radiation pressure is derived for an infinitely large drop. Our original drop size is that of the extracted film with a thickness of about one millimeter and is indeed much larger than the SAW wavelength. As a simple model, we assume the acoustic radiation pressure of the original film remains valid as the film thins near the contact line and droplets smaller than the SAW wavelength are formed. Since the thin film that breaks up into droplets is slender in aspect ratio, we also neglect the decay of the acoustic radiation pressure in the vertical direction and use the average acoustic pressure at a particular droplet to estimate its capillary pressure and diameter.

Combining Eqs. (1) and (2) with these approximations, we obtain

$$L_{n+1} = L_n + \frac{8\gamma}{\rho(1 + \alpha^2)A^2\omega^2} e^{2k_x L_n}, \quad (3)$$

such that the radius of the droplets away from the pinned film will decrease exponentially away from the pinned film with a characteristic decay length that is half of the Rayleigh decay length. If we transpose Eq. (3) so that the difference of the lengths L_{n+1} and L_n is the droplet diameter D , and L_n is equivalent to position x , then the scaling relationship for droplet size becomes $\ln(D) \propto x$ with constant of proportionality $2k_x$. Figure 2(a) shows experimental data using DI water as the working fluid at a variety of SAW powers and confirms this exponential relationship with x taken to be zero where the smallest visible droplets are seen (more details on this measurement included in the Supplemental Material [29]). Further, when the SAW amplitude is scaled away, the different data sets all collapse according to the scaling suggested in Eq. (3), as shown in Fig. 2(b). The distance $L_{\text{transition}}$, from where the smallest

visible droplets are seen to the transition region where the decay rate changes, is measured experimentally. The decay length l_M^x and the drop diameter at the transition region $D_{\text{transition}}$ are adjusted empirically but both will be compared to predicted values from our theory for the Maxwell drops.

Curiously, there are actually two sets of collapsed data with two distinct exponents in Fig. 2. For the larger droplets (at greater x), an acoustic decay constant k_x value of 6800 m^{-1} (corresponding to $l_R^x = 1/k_x = 147 \mu\text{m}$) can be extracted and it is on the same order of magnitude, though larger than the reported value for water of 1370 m^{-1} or $l_R^x = 730 \mu\text{m}$ [19]. We attribute this discrepancy to droplets coalescing prior to measurement, which occurs most dramatically for larger droplets, thus artificially increasing the slope. We estimate the acoustic pressure by assuming an amplitude A on the order of ten nanometers, consistent with past studies [30], and find $P_{\text{acoustic}} \sim 10^2\text{--}10^3 \text{ Pa}$ provides sufficient pressure to sustain droplets with diameter D on the order of tens to hundreds of microns, corresponding to the larger droplets. Thus it is clear that the larger sequence of satellite droplets are generated because of the acoustic pressure near the contact line, and the sequence of these acoustic Rayleigh drops is due to a static balance between the exponentially decaying acoustic pressure and the local capillary pressure.

The second set of collapsed data for the sequence of smaller droplets suggests that a different exponentially decaying pressure with a different decay rate must be at play closer to the original contact line. We attribute this sequence of satellite drops to the Maxwell pressure due to the electric field of the transmitted SAWs that remain on the substrate. Because of the finite wavelength λ_{SAW} of the SAW, its electric field decays in the direction normal to the surface due to field leakage both out into the gas phase and

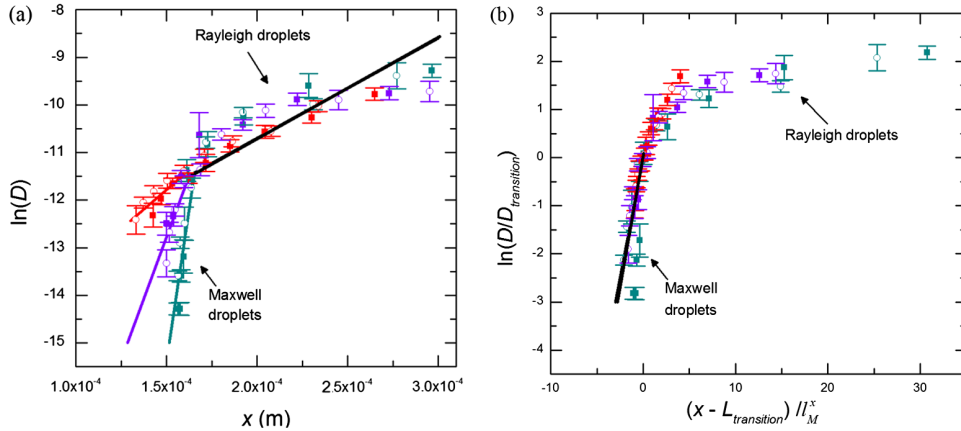


FIG. 3 (color online). (a) Plot of $\ln(D)$ as a function of x for data acquired at different contact angles along with linear curve fits. The slopes of the linear fits are equivalent to the decay constant. All units are in meters. (b) The data sets collapsed on a single plot, where $D_{\text{transition}}$ is the droplet size where the transition for the two droplet families occurs $\approx 11 \mu\text{m}$, $L_{\text{transition}}$ is the measured x location of the transition, and l_M^x is the decay length of the Maxwell pressure. Two sets of data (open and closed symbols) were acquired for each contact angle.

from the high potential region to the low potential region of the traveling wave on the substrate [31].

A Fourier expansion of the Laplace equation for the potential ϕ (see Ref. [31]) within and outside a horizontal film of thickness h , driven by a harmonic surface potential $\phi(x, y = 0) = \phi_o \cos(kx)$ by a SAW of wavelength $\lambda_{\text{SAW}} = 2\pi/k$ yields a Maxwell pressure change across the interface, averaged over one wavelength, of $P_M = \epsilon_{\text{liquid}} \phi_o^2 k^2 (\chi^2 - 1) e^X / [(-1 + e^X) + \chi(1 + e^X)]^2$, where χ is the ratio of liquid permittivity ϵ_{liquid} to air permittivity ϵ_{air} and $X = (4\pi h / \lambda_{\text{SAW}})$. An expression for large χ for large X , $P_M \sim \epsilon_{\text{liquid}} \phi_o^2 k^2 \exp(-X)$, shows that the Maxwell pressure decays exponentially with respect to the film thickness and that the Maxwell pressure becomes appreciable at $X \sim 1$, which produces a transition film thickness of $h = \lambda_{\text{SAW}}/4\pi$ or about 10.5 microns for our SAW wavelength. This is the observed value of transition droplet diameter $D_{\text{transition}}$ in Fig. 2(a) and is used to collapse the data in Fig. 2(b). This transition film height, which delineates the Maxwell drops from the Rayleigh drops, also appears in the exponent of several exponentially decaying functions in this problem. It is the decay length of the Maxwell pressure with respect to film height for large X . An expansion about $X = 1$ for large χ , which reveals a scaling of $P_M \sim \epsilon_{\text{liquid}} \phi_o^2 k^2 \exp[-0.462(X - 1)]$ with exponential factor $(e - 1)/(e + 1) \approx 0.462$, is assumed to be valid for the observed Maxwell droplets.

With a thin-film approximation, the film height of the wedge-shaped film near the contact line is $h = x \tan(\theta_c)$ where x is the tangential coordinate from the contact line. This approximation allows us to use the $X \sim 1$ flat-film Maxwell pressure to estimate the Maxwell pressure decay with respect to x , $P_M \sim \epsilon_{\text{liquid}} \phi_o^2 k^2 \exp(-x/l_M^x)$, where $l_M^x = \frac{\lambda_{\text{SAW}}}{4\pi \tan \theta_c} \frac{e+1}{e-1}$ is the Maxwell pressure decay length in the x direction. This Maxwell decay length for $\theta_c \approx 45^\circ$ is

computed to be $22.7 \mu\text{m}$, which is roughly the value obtained from Fig. 2(a) of $19.2 \mu\text{m}$ by empirical fit.

Since the tangential decay length for the Maxwell droplets is a strong function of the contact angle, we explore this wettability dependence by pretreating the substrate with trichloro(1H,1H,2H,2H-perfluoroctyl)silane via evaporation. The untreated substrate produced a contact angle of 45° while the chemical produced contact angles of 70° and 80° . As is evident in Fig. 3(a), the Rayleigh drop distribution and the transition film thickness are unaffected by the contact angle but the decay length of the Maxwell droplets is indeed a strong function of the contact angle. Inserting the scaling of $\tan \theta_c$ collapses the data for different contact angles in Fig. 3(b). We observe that when a nonwetting droplet with contact angle as high as $\theta_c \sim 120^\circ$ is subjected to a SAW, its contact angle decreases to a saturation value of approximately 85° and Maxwell nanodroplets are still generated. In general, however, the thin film field-leakage mechanism breaks down for nonwetting liquids so we do not expect Maxwell drops to form for θ_c much greater than 90° .

In addition to enhanced Maxwell stress due to field leakage for thin films, there could also be singular harmonics at contact-line wedge [21–25] that further magnifies the electric field. By seeding the solution with nanocrystals and imaging the residual crystallization on the substrate after the droplets evaporated, we were able to confirm that the rapidly decaying Maxwell pressure is strong enough to produce sub-micron droplets with extremely large capillary pressures as shown in Fig. 4 in the case of the untreated substrate with 45° contact angle. The outer rim of deposited nanocolloids corresponds to the original nanodrop size, and we estimate the corresponding capillary pressure to be $\sim 10^6 \text{ Pa}$. By reducing the wavelength and increasing the amplitude of SAW to their physical limits, pressures as high as $\sim 10^7 \text{ Pa}$, corresponding to $D \sim 10 \text{ nanometers}$,

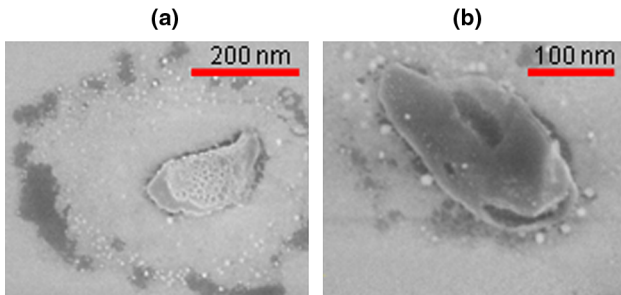


FIG. 4 (color online). Scanning electron microscope images of dried nano-droplet on an untreated substrate. DI water was seeded with 20 nanometer gold spheres for visualization.

may be achieved. This large pressure (and corresponding electric field in excess of 10^8 V/m) suggests that atomic field strengths are available at the contact-line hotspot and SAW may be able to drive new chemistry there and may explain the high ionization efficiency of SAW mass spectrometry [6–8].

D.T. wishes to acknowledge the Arthur J. Schmitt Foundation for their generous funding and Ming K. Tan for fabrication of SAW devices. In addition, D.T. would like to acknowledge the help of the Notre Dame Integrated Imaging Facility for assistance with scanning electron microscope imaging.

*Author to whom correspondence should be addressed.
hchang@nd.edu

- [1] L. Rayleigh, *Proc. London Math. Soc. s1–17*, 4 (1885).
- [2] D.P. Morgan, *Surface Acoustic Wave Filters, Second Edition: With Applications to Electronic Communications and Signal Processing* (Academic Press, Amsterdam, 2007).
- [3] B.A. Auld, *Acoustic Fields and Waves in Solids* (Robert E. Kreiger Publishing Co., Malabar, 1990), 2nd ed., Vol. I–II.
- [4] A. Ruiz and P.B. Nagy, *Ultrasonics* **42**, 665 (2004).
- [5] M. K. Tan, J.R. Friend, O. K. Matar, and L. Y. Yeo, *Phys. Fluids* **22**, 112112 (2010).
- [6] J. Ho, M. K. Tan, D.B. Go, L. Y. Yeo, J.R. Friend, and H.-C. Chang, *Anal. Chem.* **83**, 3260 (2011).
- [7] A. Qi, L. Yeo, J. Friend, and J. Ho, *Lab Chip* **10**, 470 (2010).

- [8] S. R. Heron, R. Wilson, S. A. Shaffer, D. R. Goodlett, and J. M. Cooper, *Anal. Chem.* **82**, 3985 (2010).
- [9] J. Friend and L. Y. Yeo, *Rev. Mod. Phys.* **83**, 647 (2011).
- [10] M. Kurosawa, A. Futami, and T. Higuchi, *International Conference on Solid State Sensors and Actuators, Chicago* (IEEE, Chicago, IL, 1997), Vol. 2, p. 801.
- [11] M. Kurosawa, T. Watanabe, A. Futami, and T. Higuchi, *Sens. Actuators A, Phys.* **50**, 69 (1995).
- [12] M. Alvarez, J. R. Friend, and L. Y. Yeo, *Nanotechnology* **19**, 455103 (2008).
- [13] P.K. Bhattacharjee, A.G. McDonnell, R. Prabhakar, L.Y. Yeo, and J. Friend, *New J. Phys.* **13**, 023005 (2011).
- [14] M. K. Tan, J. R. Friend, and L. Y. Yeo, *Phys. Rev. Lett.* **103**, 024501 (2009).
- [15] K. Chono, N. Shimizu, Y. Matsui, J. Kondoh, and S. Shiokawa, *Jpn. J. Appl. Phys.* **43**, 2987 (2004).
- [16] A. Qi, L. Yeo, and J. Friend, *Phys. Fluids* **20**, 074103 (2008).
- [17] Y. Luo, J.B. Pendry, and A. Aubry, *Nano Lett.* **10**, 4186 (2010).
- [18] R.V. Craster and A.V. Shanin, *Proc. R. Soc. A* **461**, 2227 (2005).
- [19] S. Shiokawa and Y. Matsui, *Mater. Res. Soc. Symp. Proc.* **360**, 53 (1994).
- [20] M. Alvarez, J. Friend, and L. Yeo, *Langmuir* **24**, 10629 (2008).
- [21] S. K. Thamida and H.-C. Chang, *Phys. Fluids* **14**, 4315 (2002).
- [22] N. Chetwani, S. Maheshwari, and H. C. Chang, *Phys. Rev. Lett.* **101**, 204501 (2008).
- [23] K. H. Kang, *Langmuir* **18**, 10318 (2002).
- [24] F. Muggele and J. Buehrle, *J. Phys. Condens. Matter* **19**, 375112 (2007).
- [25] G.I. Taylor, *Proc. R. Soc. Edinburgh, Sect. A* **280**, 1382 (1964).
- [26] P.E. Lagasse, I.M. Mason, and E.A. Ash, *IEEE Trans. Microwave Theory Tech.* **21**, 225 (1973).
- [27] X. Jia and M. de Billy, *Appl. Phys. Lett.* **61**, 2970 (1992).
- [28] T.-T. Wu, H.-T. Tang, Y.-Y. Chen, and P.-L. Liu, *IEEE Trans. Sonics. Ultrason.* **52**, 1384 (2005).
- [29] See Supplemental Material at <http://link.aps.org-supplemental/10.1103/PhysRevLett.109.224301> for additional information on droplet measurement.
- [30] M. K. Tan, J. R. Friend, and L. Y. Yeo, *Appl. Phys. Lett.* **91**, 224101 (2007).
- [31] O. Orlychenko, Y. Ye, and H.-C. Chang, *Phys. Rev. E* **57**, 5196 (1998).